

Intention-Aware Control Based on Belief-Space Specifications and Stochastic Expansion

Zengjie Zhang¹, Zhiyong Sun¹, and Sofie Haesaert¹

Abstract—This paper develops a correct-by-design controller for an autonomous vehicle interacting with opponent vehicles with unknown intentions. We use discrete-valued random variables to model unknown intentions. Based on this, we define an intention-aware control problem for an autonomous vehicle and a collection of opponent agents with epistemic uncertainty. To this end, we focus on a control objective specified in the belief space with temporal logic specifications. From this stochastic control problem, we derive a sound deterministic control problem using stochastic expansion and solve it using shrinking-horizon model predictive control. The solved intention-aware controller allows a vehicle to adjust its behaviors according to its opponents' intentions. It ensures provable safety by restricting the probabilistic risk under a desired level. We show with experimental studies that the proposed method ensures strict limitation of risk probabilities, validating its efficacy in autonomous driving cases. This work provides a novel solution for the risk-aware control of interactive vehicles with formal safety guarantees.

I. INTRODUCTION

When an autonomous vehicle interacts with other traffic participants, being aware of the intention of these participants strongly impacts the safety and reliability of prediction and decision-making in its motion planning. This has motivated the studies on *intention-aware* motion planning [1]–[3]. Fig. 1 shows an intersection case where an ego vehicle (EV) plans a left turn while avoiding collisions with opponent vehicles (OVs) and pedestrians from the opposite direction. Understanding the intentions of these opponents (e.g., moving fast or slowly) facilitates the design of a safe and flexible policy. Intention-aware motion planning has been formulated as a partially observable Markov decision process (POMDP) [4], where intentions are discrete-valued unobservable variables encoding uncertain policies [5]. Decision-making with the awareness of intentions aims at a safe policy for all assumed opponents' behaviors, rendering a challenging planning problem with complex uncertainties. Planning-based methods, such as reinforcement learning, have been applied [6]. However, planning-based methods rely on precise agent models, causing *sim-to-real* issues when models are imprecise [7]. Moreover, these solutions hardly ensure formal safety guarantees or probable risk restrictions [8]. These concerns enforce the need for an intention-aware controller that is correct by design and is

robust to modeling errors, which has not been solved yet in the literature.

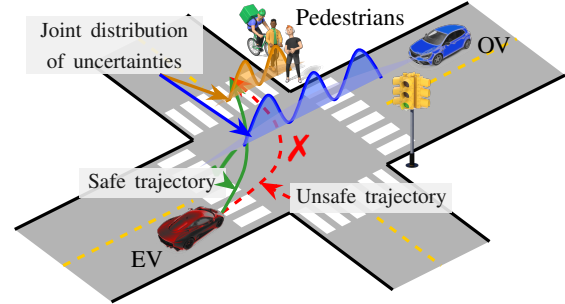


Fig. 1: An intersection case where an EV plans a collision-free left turn, aiming at a safe trajectory for the complex modeling-intention uncertainties of the OV and pedestrians. Understanding the intentions of the OV and the pedestrians helps the EV make safe and flexible decisions.

Control of autonomous agents with stochastic uncertainties has been formulated as a stochastic control problem subject to probability constraints [9]. Beyond this, formal safety guarantees have been specified as temporal logic formulas, such as Signal Temporal Logic (STL) [10] and Linear-time Temporal Logic (LTL) [11], aiming at a *risk-aware* controller that restricts risk probabilities to certain levels [12]. A stochastic control problem with formal specifications can be solved using Model Predictive Control (MPC) [13] and abstraction-based methods [14]. Belief-space specifications, such as Partially observable computation tree logic (POCTL) [15], Distribution Temporal Logic (DTL) [16], Gaussian DTL [17], and probabilistic STL [18] have been proposed to convert a stochastic control problem into a more tractable deterministic belief-space control problem [19]. Specification decomposition [20] and splitting [21] approaches improve the efficiency of solving a control problem with STL.

However, these existing control methods mainly apply to uncertainties with Gaussian or bounded-support distributions [22]. As to be addressed later, intention-aware control requires characterizing complex uncertainties with non-Gaussian or multi-modal distributions, thus remaining an open and challenging problem. An effective approach to precisely characterize nontrivial probabilistic distributions is stochastic expansion [23]. As a representative method of stochastic expansion, Polynomial Chaos Expansion (PCE) can efficiently characterize an arbitrary probabilistic model

*This work was supported by the European project SymAware under grant No. 101070802.

¹Zengjie Zhang, Zhiyong Sun, and Sofie Haesaert are with the Department of Electrical Engineering, Eindhoven University of Technology, PO Box 513, 5600 MB Eindhoven, Netherlands {z.zhang3, z.sun, s.haesaert}@tue.nl

by decomposing it to a linear combination of a finite number of orthogonal bases. It has shown advantages in robust control with non-Gaussian uncertainties [24]. Stochastic expansion mainly applies to systems with *epistemic* uncertainties [25] subject to time-invariant distributions. In this sense, stochastic expansion is promising to facilitate the closed-loop intention-aware control for epistemically uncertain systems.

This paper provides the first correct-by-design solution for intention-aware control of uncertain autonomous agents. Beyond the conventional POMDP-based intention-aware planning problem, we derive a stochastic control problem for epistemically uncertain agents with a belief-space specification. Then, we use stochastic expansion to convert this challenging stochastic control problem into a tractable deterministic control problem with an STL specification. This allows us to solve a challenging intention-aware control problem using off-the-shelf tools, such as shrinking-horizon MPC [13] based on Mixed-Integer Planning (MIP) [26]. With assumed intention models, the solved intention-aware controller allows automatic policy adjustment and ensures strict risk limitation. Two autonomous driving cases, namely an overtaking case and an intersection case, have validated the efficacy of this method.

The rest of this paper is organized as follows. Sec. II states the intention-aware control problem for an EV with multiple OVs and pedestrians. Sec. III gives the mathematical solution to this problem. Sec. IV uses two autonomous driving experimental studies to validate the efficacy of the proposed solution. Finally, Sec. V concludes the paper.

Notation: $\mathbb{R}(\mathbb{R}^+)$, $\mathbb{Z}(\mathbb{Z}^+)$ are sets of (positive) real numbers and integers, respectively. \mathbb{N} denotes natural numbers.

II. PROBLEM STATEMENT

This section states the intention-aware control problem based on the intersection case raised at the beginning of this paper, which will be mathematically solved in Sec. III.

A. Intention Awareness for the Intersection Case

The intersection case shown in Fig. 1 serves as a typical autonomous driving scenario where an EV needs to plan a safe trajectory incorporating the interaction with the other traffic participants, such as OVs and pedestrians. As an interactive participant, an OV or a pedestrian seeing the EV approaching might have various intents motivated by different driving or moving styles [27], requiring the EV to take different strategies accordingly. For example, an antagonistic OV tends to *speed up* to show a strong sense of priority. On the contrary, a cooperative OV may *slow down* to give out the priority. There might also be an ignorant OV that remains a *constant speed*, regardless of the reaction to the EV. Similarly, younger pedestrians tend to move faster than the elders. The EV must incorporate all possible intentions of these traffic participants into its motion planning to minimize the likelihood of possible collisions. In this way, the EV recognizes a participant as an *interactive* agent that proactively reacts to its presence, instead of simply

a dynamic obstacle, forming a foundation for *interaction-aware* autonomous driving [28].

Predicting the motion of a traffic participant with known models and intentions is trivial, which, however, is hardly possible in practice. Instead, it is more common that the EV only knows their possible intents but is not certain about which intents are to be realized in the future. In such a probabilistic setting, the EV can understand the behaviors of the other participants as random signals and plan a trajectory that ensures safety in a probabilistic sense. Specifically, using a random signal $\mathbf{s} := s_0 s_1 \cdots$ to denote the joint positions of all traffic participants and an STL specification ϕ (see Appx.-A for the details of STL) to describe the safe intersection task, we aim to solve a control policy for the EV to ensure a constrained success probability $P(\mathbf{s} \models \phi) > 1 - \epsilon$, meaning that the intersection task should be accomplished with a minimal probability $1 - \epsilon$, where $\epsilon \in (0, 1)$ is a predefined risk level. This renders a safety-critical *risk-, intention-, and interaction-aware* policy by imposing a strict limitation on the risk probability $P(\mathbf{s} \not\models \phi) \leq \epsilon$. We will give the complete problem statement in Sec. II-C after introducing the uncertain vehicle models in the following subsection.

B. Models with Epistemic Uncertainty

An autonomous vehicle is typically described as a nonlinear bicycle model [29] as outlined in Appx.-B. This model serves as a special deterministic instance of a POMDP involved in [5], [30] but without random uncertainty in state transition and observation. Different from the conventional POMDP models, we explore a form of random uncertainty arising from continuous random parameters of a vehicle model, like vehicle length or control bias, as elucidated in Appx.-C. Similar uncertain models with random parameters have also been used to describe the group behavior of pedestrians [31]. Together with discrete-valued random intentions introduced in Sec. II-A, a type of uncertain model subject to both continuous and discrete random variables is addressed for an OV or a group of pedestrians, or an *opponent*. As a result, the positions of these opponents rendered by their random models form a joint random signal subject to a complex, typically a multi-modal distribution, as depicted in Fig. 1. Quantifying such complex uncertainty poses a challenge to solving the intention-aware control problem.

Even the exact values of the random parameters and intentions are not known, their distributions can be obtained using empirical or inference methods [32], [33]. The uncertainty brought up by random parameters is referred to as *epistemic uncertainty* since their distributions are time-invariant and can be learned with sufficient observation data [25]. On the contrary is *aleatory* uncertainty that can never be precisely characterized by a time-invariant probabilistic distribution nor observation data, such as the random noise of a stochastic system [34]. Stochastic expansion methods, such as PCE, have provided powerful tools to precisely characterize the propagation of complex distributions [23]. The characterization has proved to be tractable for time-invariant distributions. In this sense, PCE shows great potential in solving

the intention-aware control problem that requires the precise quantification of epistemic uncertainty.

C. Intention-Aware Control with Formal Specifications

Based on the intention and behavioral models above, the intention-aware control problem of an EV interacting with multiple opponents (OVs or groups of pedestrians) is formulated as follows.

Problem 1: Consider an EV with a deterministic model and multiple opponents with uncertain models. Each opponent model has a continuous-valued random parameter $\theta \sim p_\theta$ and a discrete-valued random intention $\iota \sim p_\iota$, where p_θ is a multi-dimensional joint probability density function (PDF) and p_ι is a distribution. Solve a controller for the EV, such that a random signal $\mathbf{s} := s_0 s_1 \dots$ encoding the joint positions of all traffic participants satisfies a predefined STL specification φ at a minimal probability level $P(\mathbf{s} \models \varphi) > 1 - \varepsilon$, with $\varepsilon \in (0, 1)$. \square

In Problem 1, it is reasonable to consider a deterministic model for the EV since its intention does not need to be considered. Besides, obtaining a well-identified model for the EV is trivial, making it unnecessary to incorporate parametric uncertainties [35]. Thus, the main difficulty of solving Problem 1 lies in characterizing the complex joint distribution of the uncertainty brought up by the random intention ι and parameters θ of all opponents. In the following section, we will give a mathematical solution to Problem 1 by leveraging stochastic expansion methods.

III. MAIN METHOD

This section provides a mathematical solution to Problem 1, where we consider a general setting of autonomous agents with epistemic uncertainty and belief-space specifications. Then, an MPC solution ensuring provable risk restriction is obtained.

A. Vehicle Models with Random Parameters

We consider a traffic system containing a deterministic ego agent (EA) and $M \in \mathbb{Z}^+$ stochastic opponent agents (OAs), positioning Problem 1 in a generic context. Corresponding to the intersection case in Fig. 1, the EA refers to the EV that performs the turning task, and an OA is either an OV or a group of pedestrians. We describe the EA as the following discrete-time deterministic dynamic model [35],

$$\text{EA} : \begin{cases} x_{k+1} = Ax_k + Bu_k + d_k, \\ y_k = Cx_k, \end{cases} \quad (1)$$

where $x_k \in \mathbf{X} \subseteq \mathbb{R}^n$, $u_k \in \mathbf{U} \subseteq \mathbb{R}^m$, $d_k \in \mathbf{D} \subseteq \mathbb{R}^d$, and $y_k \in \mathbf{Y} \subseteq \mathbb{R}^l$ are the state, the control input, the external input, and the measurement output of the EA, respectively, at time $k \in \mathbb{N}$, and $A \in \mathbb{R}^{n \times n}$, $B \in \mathbb{R}^{n \times m}$, $C \in \mathbb{R}^{l \times n}$ are constant matrices, where $n, m, l \in \mathbb{Z}^+$. Additionally, d_k for $k \in \mathbb{N}$ is a bounded external input denoting the disturbance or modeling errors of the EA. Assume a deterministic model for EA is common in practical scenarios [35].

The EA model in Eq. (1) is a generic form of the linearized deterministic model in Appx.-B. With a deterministic initial state $x_0 \in \mathbb{R}^n$, EA generates a deterministic observation trajectory $\mathbf{y} := y_0 y_1 y_2 \dots$.

The OAs have the following stochastic models [36]

$$\text{OA}_j : \begin{cases} z_{j,k+1} = F_j(\theta_j)z_{j,k} + G_j(\theta_j)v_{j,k}, \\ w_{j,k} = H_j(\theta_j)z_{j,k}, \end{cases} \quad (2)$$

for $j \in \mathcal{M} = \{1, 2, \dots, M\}$, where $z_{j,k} \in \mathbf{Z}_j \subseteq \mathbb{R}^{p_j}$, $v_{j,k} \in \mathbf{V}_j \subseteq \mathbb{R}^{q_j}$, and $w_{j,k} \in \mathbf{W}_j \subseteq \mathbb{R}^{r_j}$ are the state, the control input, and the observation of OA_j , for $j \in \mathcal{M}$, where $p_j, q_j, r_j \in \mathbb{Z}^+$, $F_j(\theta_j) \in \mathbb{R}^{p_j \times p_j}$, $G_j(\theta_j) \in \mathbb{R}^{p_j \times q_j}$, and $H_j(\theta_j) \in \mathbb{R}^{r_j \times p_j}$ are uncertain matrices dependent on a random parameter $\theta_j \in \mathbb{R}^{t_j}$ subject to a t_j -dimensional joint probabilistic density function (PDF) p_{θ_j} , with $t_j \in \mathbb{Z}^+$. We assume the elements of θ_j are independent and identically distributed (i.i.d) random variables defined on a Hilbert space $\mathcal{L}^2(\Theta, \mathcal{F}, P)$, where Θ is a probability space, \mathcal{F} is a σ -algebra defined on Ω , P is a probability measure. Thus, all random variables in θ_j have finite second-order moments. Such models with parametric uncertainties have been commonly used [36].

Note that Eq. (2) allows a heterogeneous setting of the OAs which may have different parameters F_j , G_j , and H_j over $j \in \mathcal{M}$. The OA model in Eq. (10) is a generic form of the linearized stochastic model in Appx.-C. With a random initial state $z_{j,0} \sim p_{z_{j,0}}$ with $p_{z_{j,0}}$ being a p_j -dimensional joint PDF, each OA generate a stochastic observation trajectory $\mathbf{w}_j := w_{j,0} w_{j,1} w_{j,2} \dots$.

B. Random Intentions

For each OA_j , $j \in \mathcal{M}$, we define an discrete-valued intention variable ι_j sampled from a finite intent set I_j with a probabilistic distribution p_{ι_j} . Based on this, we assume that OA_j is controlled by the following general policy,

$$v_{j,k} := \sum_{i=1}^M K_{i,j}(\iota_j) w_{i,k} + L_j(\iota_j) \tau_{j,k}, \quad (3)$$

where $K_{i,j} : I_j \rightarrow \mathbb{R}^{q_j \times r_i}$ for $i \in \mathcal{M}$ is a feedback control gain, $\tau_{j,k} \in \mathbf{T}_j \subseteq \mathbb{R}^{q_j}$ is a predefined feedforward control input for $k \in \mathbb{N}$, and $L_j : \mathbb{R} \rightarrow \mathbb{R}^{q_j \times q_j}$ is a feedforward control gain. Eq. (3) defines a representative control policy that covers feedback control, feedforward control, and interaction with other OAs. Substituting Eq. (3) to Eq. (2), we obtain the closed-loop dynamic model of OA_j as

$$z_{j,k+1} = \sum_{i=1}^M \tilde{F}_{i,j}(\theta_j, \iota_j) z_{i,k} + \tilde{G}_j(\theta_j, \iota_j) \tau_{j,k}, \quad (4)$$

where $\tilde{F}_{i,j}(\theta_j, \iota_j) := (F_j(\theta_j) + G_j(\theta_j)K_{i,j}(\iota_j))H_j(\theta_j)$ for $i \in \mathcal{M}$ and $\tilde{G}_j(\theta_j, \iota_j) := G_j(\theta_j)L_j(\iota_j)$. Thus, the closed-loop dynamic models of the OAs can be compactly written as

$$\text{OAs(closed loop)} : \begin{cases} z_{k+1} = \mathbf{F}(\eta)z_k + \mathbf{G}(\eta)\tau_k, \\ w_k = \mathbf{H}(\eta)z_k, \end{cases} \quad (5)$$

where $z_k := [z_{1,k}^\top \dots z_{M,k}^\top]^\top \in \mathbf{Z} \subseteq \mathbb{R}^p$, $w_k := [w_{1,k}^\top \dots w_{M,k}^\top]^\top \in \mathbf{W} \subseteq \mathbb{R}^r$, and $\tau_k := [\tau_{1,k}^\top \dots \tau_{M,k}^\top]^\top \in \mathbf{T} \subseteq \mathbb{R}^q$ denote the joint state, output, and feedforward control of the OAs, respectively, where $p := \sum_{j=1}^M p_j$, $\mathbf{Z} := \prod_{j=1}^M \mathbf{Z}_j$, $q := \sum_{j=1}^M q_j$, $\mathbf{T} := \prod_{j=1}^M \mathbf{T}_j$, $r := \sum_{j=1}^M r_j$, and $\mathbf{W} := \prod_{j=1}^M \mathbf{W}_j$. $\eta := [\theta_1^\top \dots \theta_M^\top \iota_1 \dots \iota_M]^\top$ is a joint random variable containing

the uncertain parameters θ_j and intentions ι_j of all OAs, and $\mathbf{F}(\eta) \in \mathbb{R}^{p \times p}$, $\mathbf{G}(\eta) \in \mathbb{R}^{r \times q}$, and $\mathbf{H}(\eta) \in \mathbb{R}^{r \times p}$ are partitioned matrices with $\tilde{F}_{i,j}(\theta_j, \iota_j)$ being the (j, i) partition of $\mathbf{F}(\eta)$, $\tilde{G}_j(\theta_j, \iota_j)$ being the (j, j) partition of $\mathbf{G}(\eta)$, and $H_j(\theta_j)$ being the (j, j) partition of $\mathbf{H}(\eta)$, for $i, j \in \mathcal{M}$. All other partitions of these matrices are zeros. The joint output of the OAs is denoted as $\mathbf{w} := w_0 w_1 w_2 \dots$.

Since the random parameters $\theta_1, \dots, \theta_M$ are continuous-valued but the random intentions ι_1, \dots, ι_M are discrete-valued, the joint uncertainty η may be subject to a complex multi-modal distribution, as illustrated in Fig. 1. However, the uncertainty is epistemic due to its time-invariant joint distribution, allowing stochastic expansion to precisely characterize the propagation of the OA models. We will elaborate on this in Sec. III-E.

C. Probabilistic Constraints and Belief-Space Specifications

In practice, agents are assigned physical constraints for given control objectives. For the agents defined in Sec. III-A, a joint constraint has the following probabilistic form,

$$P(\gamma^\top w_k \leq \beta - \alpha^\top y_k) \geq 1 - \varepsilon, \quad k \in \mathbb{N}, \quad (6)$$

where $y_k \in \mathbb{R}^l$ and $w_k \in \mathbb{R}^r$ are the observations of the EA and the OAs at time k given by Eq. (1) and Eq. (5), $\alpha \in \mathbb{R}^r$, $\beta \in \mathbb{R}$, and $\gamma \in \mathbb{R}^r$ are constant coefficients, and $\varepsilon \in [0, 1]$ is a provable risk restriction. The constraint Eq. (7) implies a quantified risk restriction. If w_k is Gaussian for all $k \in \mathbb{N}$, according to [37], the probabilistic constraint Eq. (6) is equivalent to,

$$\alpha^\top y_k + \gamma^\top \mu_{w_k} + \kappa_\varepsilon \sqrt{\gamma^\top \Sigma_{w_k} \gamma} - \beta \leq 0, \quad (7)$$

where $\mu_{w_k} \in \mathbb{R}^r$ and $\Sigma_{w_k} \in \mathbb{R}^{r \times r}$ are the expected value and the covariance of w_k , respectively, and $\kappa_\varepsilon = \Psi^{-1}(1 - \varepsilon)$ is a scalar with Ψ being the cumulative probability function of the normal distribution. However, the equivalence between Eq. (6) and Eq. (7) does not hold if w_k is non-Gaussian, for which conservativeness is inevitably introduced. Consider that w_k has finite statistic moments of all orders. Let $\mathcal{D}(\mu_{w_k}, \Sigma_{w_k})$ be the set of all random variables that have the same expected value and covariance as w_k . Then, the following constraint,

$$\inf_{\omega \in \mathcal{D}(\mu_{w_k}, \Sigma_{w_k})} P(\gamma^\top \omega \leq \beta - \alpha^\top y_k) \geq 1 - \varepsilon, \quad k \in \mathbb{N}, \quad (8)$$

is equivalent to Eq. (7) but with $\kappa_\varepsilon = \sqrt{(1 - \varepsilon)/\varepsilon}$ [37]. Note that Eq. (8) is conservative to Eq. (6) due to the inf operator. Let $\mathcal{B}^r := \mathbb{R}^r \times \mathbf{S}^r$ be a belief space of r -dimensional random variables that have known first- and second-order moments, where $\mathbf{S}^r \subset \mathbb{R}^{r \times r}$ is the set of all positive semi-definite matrices, such that $(\mu_{w_k}, \Sigma_{w_k}) \in \mathcal{B}^r$, $\forall k \in \mathbb{N}$. Then, Eq. (7) serves as an inequality constraint defined on the belief space \mathcal{B}^r . In this way, we build a connection between probabilistic constraints and belief-space inequalities, that is, any probabilistic constraint in the form of Eq. (6) corresponds to a sound belief-space inequality as Eq. (7).

Now, we extend the belief-space inequalities as Eq. (7) into belief-space formal specifications as follows.

Definition 1 (Distribution Signal Temporal Logic (DSTL)): For random signals \mathbf{y} from Eq. (1) and \mathbf{w} from Eq. (5), a DSTL formula φ defined over the joint random signal $(\mathbf{y}, \mathbf{w}) := (y_0, w_0)(y_1, w_1) \dots$ has the following inductively defined syntax,

$$\varphi := \top \mid (\mathbf{v}, \varepsilon) \mid \neg \varphi \mid \varphi_1 \wedge \varphi_2 \mid \varphi_1 \mathbf{U}_{[a,b]} \varphi_2,$$

where φ , φ_1 and φ_2 are DSTL formulas, $(\mathbf{v}, \varepsilon)$ is a belief-space predicate associated with a mapping $g_\varepsilon : \mathbb{R}^l \times \mathcal{B}^r \rightarrow \mathbb{R}$ via $(\mathbf{v}, \varepsilon) := \begin{cases} \top, & g_\varepsilon(y_k, (\mu_{w_k}, \Sigma_{w_k})) \leq 0 \\ \neg \top, & g_\varepsilon(y_k, (\mu_{w_k}, \Sigma_{w_k})) > 0 \end{cases}$, for a given time $k \in \{0, 1, \dots, N\}$, where g_ε is defined as the left hand of the inequality Eq. (7), and $\mathbf{U}_{[a,b]}$ is the *until* operator bounded with time interval $[a, b]$, where $a, b \in \mathbb{N}$ and $a \leq b$. We define the *disjunction*, *eventually*, and *always* operators as $\varphi_1 \vee \varphi_2 := \neg(\neg \varphi_1 \wedge \neg \varphi_2)$, $\mathbf{F}_{[a,b]} \varphi := \top \mathbf{U}_{[a,b]} \varphi$, $\mathbf{G}_{[a,b]} \varphi := \neg(\top \mathbf{U}_{[a,b]} \neg \varphi)$. The semantics of the DSTL $((\mathbf{y}, \mathbf{w}), k) \models \varphi$ are recursively defined as follows,

$$\begin{aligned} ((\mathbf{y}, \mathbf{w}), k) &\models (\mathbf{v}, \varepsilon) \leftrightarrow g_\varepsilon(y_k, (\mu_{w_k}, \Sigma_{w_k})) \leq 0, \\ ((\mathbf{y}, \mathbf{w}), k) &\models \neg \varphi \leftrightarrow \neg(((\mathbf{y}, \mathbf{w}), k) \models \varphi), \\ ((\mathbf{y}, \mathbf{w}), k) &\models \varphi_1 \wedge \varphi_2 \leftrightarrow ((\mathbf{y}, \mathbf{w}), k) \models \varphi_1 \wedge ((\mathbf{y}, \mathbf{w}), k) \models \varphi_2, \\ ((\mathbf{y}, \mathbf{w}), k) &\models \varphi_1 \vee \varphi_2 \leftrightarrow ((\mathbf{y}, \mathbf{w}), k) \models \varphi_1 \vee ((\mathbf{y}, \mathbf{w}), k) \models \varphi_2, \\ ((\mathbf{y}, \mathbf{w}), k) &\models \mathbf{F}_{[a,b]} \varphi \leftrightarrow \exists k' \in [k+a, k+b], ((\mathbf{y}, \mathbf{w}), k') \models \varphi, \\ ((\mathbf{y}, \mathbf{w}), k) &\models \mathbf{G}_{[a,b]} \varphi \leftrightarrow \forall k' \in [k+a, k+b], ((\mathbf{y}, \mathbf{w}), k') \models \varphi, \\ ((\mathbf{y}, \mathbf{w}), k) &\models \varphi_1 \mathbf{U}_{[a,b]} \varphi_2 \leftrightarrow \exists k' \in [k+a, k+b], \\ &\quad \text{s.t. } ((\mathbf{y}, \mathbf{w}), k') \models \varphi_2, \text{ and } \forall k'' \in [k, k'], ((\mathbf{y}, \mathbf{w}), k'') \models \varphi_1. \end{aligned}$$

For $k=0$, the symbol k is omitted, rendering $(\mathbf{y}, \mathbf{w}) \models \varphi$. \square

Each DSTL predicate renders a belief-space inequality equivalent to a sound probabilistic constraint like Eq. (8), building a connection between DSTL and probabilistic constraints. DSTL can be recognized as a generalization of STL (See Appx.-A) to belief spaces or an extension of DTL [16] or Gaussian DTL [17] to real-valued signals.

D. Intention-Aware Model Predictive Control

This subsection reformulates the original motion planning problem in Problem 1 as a control problem to be solved using an MPC method.

Problem 2 (Intention-Aware Formal Control):

For the agent and intention models defined above, solve a history- and intention-dependent controller $\pi : \mathbf{Y}_+ \times \prod_{j=1}^M \mathcal{P}_j \rightarrow \mathbf{U}$ for the EA, where \mathbf{Y}_+ is the set of all finite observation sequences and \mathcal{P}_j is the space of all possible distributions of OA $_j$'s intention, $j \in \mathcal{M}$, such that the observation trajectories \mathbf{y} and \mathbf{w} satisfy a predefined DSTL formula, i.e., $(\mathbf{y}, \mathbf{w}) \models \varphi$. \square

Compared to the original Problems 1, Problem 2 uses a DSTL formula to specify the task, instead of an STL specification. This problem can be solved using a *shrinking-horizon* MPC method [13]. For any time $k \in \{0, 1, \dots, N-1\}$ with history measurements $y_0 y_1 \dots y_k \in \mathbf{Y}^+$, one aims to solve

the following optimization problem,

$$\min_{\tilde{\mathbf{u}}_k} \sum_{i=0}^{N-k-1} \tilde{\mathbf{u}}_{i|k}^\top R \tilde{\mathbf{u}}_{i|k} \quad (9a)$$

$$\text{s.t. } \tilde{x}_{i+1|k} = A\tilde{x}_{i|k} + B\tilde{u}_{i|k}, \quad (9b)$$

$$\tilde{\mathbf{u}}_{i|k} \in \mathbf{U}, \quad \forall i \in \{0, 1, \dots, N-k-1\}, \quad (9c)$$

$$\tilde{y}_{i+k|k} = C\tilde{x}_{i|k}, \quad \forall i \in \{0, 1, \dots, N-k\}, \quad (9d)$$

$$\tilde{y}_{r|k} = y_r, \quad \forall r \in \{0, 1, \dots, k\}, \quad (9e)$$

$$(\tilde{\mathbf{y}}_k, \mathbf{w}) \models \varphi, \quad (9f)$$

where $R \in \mathbb{R}^{m \times m}$ is a cost matrix, $\tilde{\mathbf{x}}_k := \tilde{x}_{0|k} \tilde{x}_{1|k} \dots \tilde{x}_{N-k|k}$, $\tilde{\mathbf{u}}_k := \tilde{u}_{0|k} \tilde{u}_{1|k} \dots \tilde{u}_{N-k-1|k}$, and $\tilde{\mathbf{y}}_k := \tilde{y}_{0|k} \tilde{y}_{1|k} \dots \tilde{y}_{N|k}$ are decision variables for the state, the input, and the output at time k , $\mathbf{U} \subseteq \mathbb{R}^m$ is a control constraint set, and $\mathbf{w} := w_0 w_1 \dots w_N$ is the measurement trajectory of the OAs generated by Eq. (2) with an intention-dependent policy in (3). Having solved $\tilde{\mathbf{u}}_k$, one can apply its first element $\tilde{u}_{0|k}$ to the EA (1) as the control input. The solved controller is robust to the external input d_k in Eq. (1).

Remark 1 (Joint Uncertainty): Eq. (9) renders a stochastic control problem due to the belief-space specification φ . It is challenging to solve due to the complex joint uncertainty brought up by the random initial condition $z_{j,0}$, the unknown parameter θ_j , and the uncertain intention ι_j of all OAs $j \in \mathcal{M}$. A solution facilitated by PCE is presented as follows.

E. Control Solution by Stochastic Expansion

PCE as a typical stochastic expansion approach, allows the stochastic parameters \mathbf{F} , \mathbf{G} , and \mathbf{H} in Eq. (5) to be approximated as $\mathbf{F} = \sum_{i=0}^{L-1} \hat{\mathbf{F}}_i \Phi_i$, $\mathbf{G} = \sum_{i=0}^{L-1} \hat{\mathbf{G}}_i \Phi_i$, and $\mathbf{H} = \sum_{i=0}^{L-1} \hat{\mathbf{H}}_i \Phi_i$, where $L \in \mathbb{Z}$ is a predefined finite expansion order, $\Phi = \{\Phi_0 \Phi_1 \dots \Phi_{L-1}\}$ is a series of orthogonal polynomial bases with $\Phi_0 := 1$, and $\hat{\mathbf{F}}_i \in \mathbb{R}^{p \times p}$, $\hat{\mathbf{G}}_i \in \mathbb{R}^{p \times q}$, and $\hat{\mathbf{H}}_i \in \mathbb{R}^{r \times p}$, for $i \in \{0, 1, \dots, L-1\}$, are PCE coefficients which can be calculated using off-the-shelf tools [38]. The approximation precision is guaranteed in a Hilbert sense [39]. Similar expansion can also be performed to z_k and w_k , with $z_k = \sum_{i=0}^{L-1} \hat{z}_{k,i} \Phi_i$, and $w_k = \sum_{i=0}^{L-1} \hat{w}_{k,i} \Phi_i$, for $k \in \mathbb{N}$, where $\hat{z}_{k,i} \in \mathbb{R}^p$ and $\hat{w}_{k,i} \in \mathbb{R}^r$ are expansion coefficients of z_k and w_k , respectively. Applying the above expansions to Eq. (5), we have the following PCE-based dynamic model,

$$\text{OAs (PCE model)} : \begin{cases} \hat{z}_{k+1} = \hat{\mathbf{F}} \hat{z}_k + \hat{\mathbf{G}} \tau_k, \\ \hat{w}_k = \hat{\mathbf{H}} \hat{z}_k, \end{cases} \quad (10)$$

where $\hat{z}_k = [\hat{z}_{k,0}^\top \dots \hat{z}_{k,L-1}^\top]^\top$ and $\hat{w}_k = [\hat{w}_{k,0}^\top \dots \hat{w}_{k,L-1}^\top]^\top$ are PCE coefficients, $\hat{\mathbf{F}} \in \mathbb{R}^{pL \times pL}$ has $\sum_{i=0}^{L-1} \hat{\mathbf{F}}_i \Psi_{ijr}$ as its j, r -th partition, where $\Psi_{ijr} = E(\Phi_i \Phi_j \Phi_r) / E(\Phi_j^2)$, $j, r \in \{0, 1, \dots, L-1\}$, $\hat{\mathbf{G}} = [\hat{\mathbf{G}}_0^\top \hat{\mathbf{G}}_1^\top \dots \hat{\mathbf{G}}_{L-1}^\top]^\top \in \mathbb{R}^{pL \times q}$, and $\mathbf{H} = \text{diag}(\hat{\mathbf{H}}_0 \hat{\mathbf{H}}_1 \dots \hat{\mathbf{H}}_{L-1}) \in \mathbb{R}^{rL \times pL}$. The PCE-based model in Eq. (10) is a generic form of the PCE-based vehicle model in Appx.-C.

Note that a deterministic PCE-based model as Eq. (10) only exists for systems with *epistemic* uncertainty η which has a time-invariant joint distribution p_η . It describes a deterministic dynamic model of the PCE coefficients \hat{z}_k and \hat{w}_k which can precisely quantify the statistics of z_k and w_k

at any time $k \in \mathbb{Z}$. For example, the expected value μ_{w_k} and the covariance Σ_{w_k} of w_k read

$$\mu_{w_k} = \hat{w}_{k,0}, \quad \Sigma_{w_k} = \sum_{i=1}^{L-1} \hat{w}_{k,i} \hat{w}_{k,i}^\top E(\Phi_i^2). \quad (11)$$

This allows the original stochastic problem in Eq. (9) to be solved via the following deterministic problem,

$$\min_{\tilde{\mathbf{u}}_k} \sum_{i=0}^{N-k-1} \tilde{\mathbf{u}}_{i|k}^\top R \tilde{\mathbf{u}}_{i|k} \quad (12a)$$

$$\text{s.t. } \tilde{x}_{i+1|k} = A\tilde{x}_{i|k} + B\tilde{u}_{i|k}, \quad (12b)$$

$$\tilde{\mathbf{u}}_{i|k} \in \mathbf{U}, \quad \forall i \in \{0, 1, \dots, N-k-1\} \quad (12c)$$

$$\tilde{y}_{i+k|k} = C\tilde{x}_{i|k}, \quad \forall i \in \{0, 1, \dots, N-k\}, \quad (12d)$$

$$\tilde{y}_{r|k} = y_r, \quad \forall r \in \{0, 1, \dots, k\}, \quad (12e)$$

$$\hat{z}_{i+1} = \hat{\mathbf{F}} \hat{z}_i + \hat{\mathbf{G}} \tau_i, \quad \forall i \in \{0, 1, \dots, N-1\}, \quad (12f)$$

$$\hat{w}_i = \hat{\mathbf{H}} \hat{z}_i, \quad \forall i \in \{0, 1, \dots, N\}, \quad (12g)$$

$$\rho^\Psi(\omega_k) > 0, \quad (12h)$$

where $\omega_k := \omega_{0|k} \omega_{1|k} \dots \omega_{N|k}$ is a deterministic signal with $\omega_{i|k} := [\tilde{y}_{i|k}^\top \hat{w}_{i|k}^\top]^\top$, for $i \in \{0, 1, \dots, N\}$ and Ψ is an STL formula (see Appx.-A) ensuring $\rho^\Psi(\omega_k) > 0 \rightarrow (\tilde{\mathbf{y}}_k, \mathbf{w}) \models \varphi$, which can be straightforwardly determined by substituting the approximation in Eq. (11) to each belief-space predicate of the DSTL formula φ . Eq. (12) allows solving the challenging Problem 2 using off-the-shelf tools such as MIP [26].

Remark 2 (Computational Complexity): The computational complexity of Eq. (12) for each time $k \in \{0, 1, \dots, N\}$ is in general exponential to the number of binary variables brought up by the specification constraint (12h), according to [26]. Since all history observation variables $\tilde{y}_{r|k}$ for $r \in \{0, 1, \dots, k\}$ are constrained by equalities (12e) without binary variables, the number of binary variables can be estimated by $O(n(N-k))$, where n is the maximal number of STL predicates specified for a specific time from k to N . In other words, n depends on the complexity of the task. In this sense, the total computational complexity of problem Eq. (12) at time $k \in \{0, 1, \dots, N\}$ is estimated as $O(2^{n(N-k)})$.

Computational complexity has been a common and open problem for formal control methods. To solve this problem, methods of specification decomposition [40] and timing split [21] have been proposed to reduce the task complexity (quantified by n in Remark 2) and horizon (N in Remark 2), respectively. Given these methods, resolving computational complexity for intention-aware control is beyond the scope of this work and will be studied in future work.

IV. EXPERIMENTAL STUDIES

This section uses two autonomous driving cases to show the efficacy of our intention-aware control method. The code of the studies can be found at <https://github.com/zhang-zengjie/IntentAware/tree/release>. All experiments are programmed in Python, solved using the *stlpy* [26] and the *chaospy* [41] toolboxes, and run on a ThinkPad Laptop with an Intel® Core i7-10750H CPU. A video demonstration of the experimental studies is available at https://youtu.be/Pvaj_e2h1Y0.

A. Case I: Overtaking

We use an overtaking case to show that an intention-aware controller allows an agent to automatically adjust its behavior according to the intents of its opponent. As shown in Fig. 2, an EV needs to overtake an OV without causing collisions. The EV and the OV are described as deterministic and stochastic linearized bicycle models (see Appx.-B and -C), respectively. The OV has an unknown length l and a random control offset δ (see Appx.-C), both sampled from non-Gaussian distributions, with l from a uniform distribution $\mathcal{U}(3.99, 4.01)$ and δ from a truncated Gaussian distribution $\mathcal{N}(0, 0.1^2)_{[-0.1, 0.1]}$. We consider three different scenarios where the OV intends to *slow down*, *speed up*, or *switch to the fast lane*, corresponding to *cooperative*, *antagonistic*, and *ignorant* driving styles, respectively.

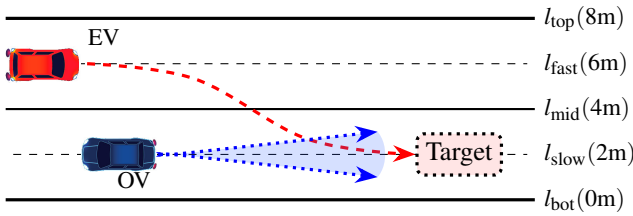


Fig. 2: The overtaking case, where an EV in the fast lane should switch to the slow lane and overtake an OV within a finite time (the dashed and arrowed trajectory). The area in front of the OV bounded by two dotted arrows denotes its joint modeling-intention uncertainty at a certain risk level.

The overtaking task is first described as natural language. *The EV eventually switches to the slow lane and drives in front of the OV at a maximal risk level 0.05 (95% success probability), if the OV does not switch to the fast lane or exceed a speed limit $v_{lim} = 12\text{m/s}$ (in an average sense). Meanwhile, the EV should always drive inside the lanes and keep a minimal distance with the OV, $d_{safe,x} = 4\text{m}$ longitudinally and $d_{safe,y} = 2\text{m}$ latitudinally, at a maximal risk level 0.05 (95% safe).* Then, the task is specified using a DSTL formula for the stochastic model of the OV and converted to an STL formula for its PCE model (See Appx.-D). We solve the MPC problem in Eq. (12) with a discrete-time $\Delta t = 1\text{s}$ and a finite control horizon with length $N = 15$. The control cost is set as $R = \text{diag}(10^4, 10^{-6})$ to penalize over-steering but encourage speed adjustment. Each time we solve Eq. (12), we update the linearized vehicle models using their current states to reduce the impact of linearization errors.

The resulting trajectories of the EV and the OV with various intentions are shown in Fig. 3. We can see that the EV changes its behaviors when the intention of the OV varies. As shown in Fig. 3a), when the OV intends to keep a constant speed and is not expected to exceed the speed limit v_{lim} , the EV performs a successful overtake. When the OV intends to speed up as to exceed the speed limit v_{lim} , as shown in Fig. 3b), the EV decides to give up overtaking and maintains its current speed instead. When the OV intends to perform an

aggressive lane-switching, as shown in Fig. 3c), the EV slows down to avoid potential collisions with the OV. Meanwhile, the EV always remains in the lanes. A 100-time Monte Carlo sampling results in zero collision cases, indicating a risk level lower than 0.05. Therefore, the behavior of the EV satisfies the overtaking task specification for all three scenarios despite the linearization errors, implying the efficacy of the proposed intention-aware control method.

In each scenario of this case study, we assume that the OV has a certain and unchanged intention known by the EV, which is not always practical in reality. In practice, the EV usually need to infer the OV's intention from its history behavior [32]. Moreover, practical vehicles may reveal different intentions in sequence. In such cases, the EV should not only infer the sequential intentions of the OV but also estimate the time horizons of these intentions. This renders an interesting but challenging sequential intention-aware control problem which is expected to be investigated in future work.

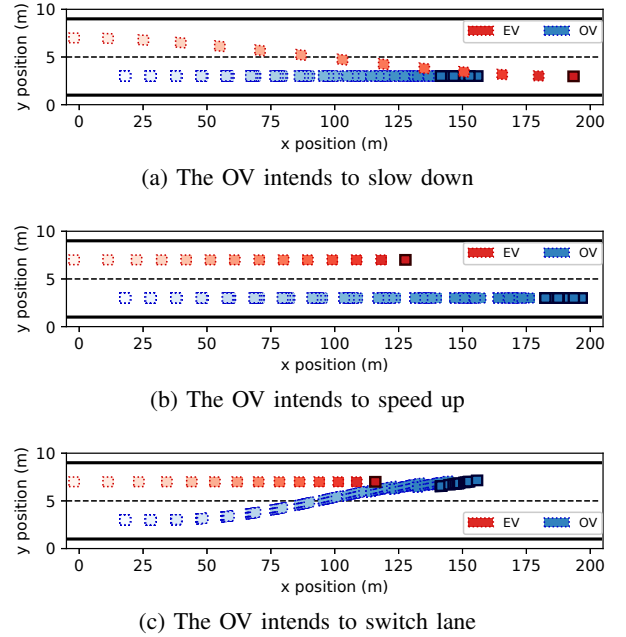


Fig. 3: The trajectories of the EV and the OV with different certain intentions. The OV trajectories result from 100 times Monte Carlo sampling of its random parameters l and δ .

The computation time per step for all three scenarios is presented in Fig. 4. All scenarios show exponentially decaying computation time as the step increases, consistent with our analysis in Remark 2. The *slow down* (for OV) scenario involves heavier computations than the other two since it is the only one that leads to successful EV overtaking. Overall, the overtaking task is sufficiently simple such that all computations have been accomplished within 0.2 s, much smaller than the discrete sampling time 1 s. This indicates that our method is promising to be deployed to practical vehicles with real-time performance requirements.

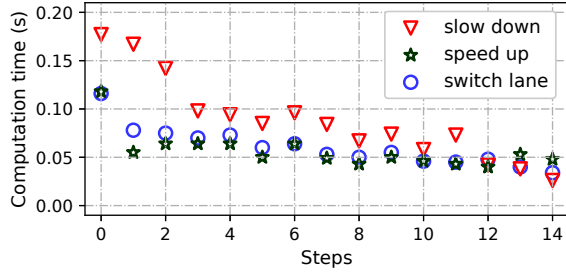


Fig. 4: The computation time per step (Case I).

B. Case II: Intersection

In this study, we use the intersection case raised in Sec. I (See Fig. 1) to show how an intention-aware controller ensures risk restriction for uncertain intentions. Similar to Sec. IV-A, the EV and the OV are described using deterministic and stochastic linearized bicycle models, respectively. The OV has an unknown length and a random control offset sampled from a uniform distribution $\mathcal{U}(3.59, 3.61)$ and a Gaussian distribution $\mathcal{N}(0, 0.01^2)$, respectively. Besides, we use a similar stochastic vehicle model, with an unknown length sampled from $\mathcal{U}(0.490, 0.501)$ and a random control offset sampled from $\mathcal{N}(0, 0.01^2)$, to denote the distributional behavior of a group of pedestrians. We consider an uncertain intention of the OV with possible intents $\{\text{speed up, constant speed, slow down}\}$, corresponding to *antagonistic*, *ignorant*, and *cooperative* driving strategies, respectively. This intention is subject to a uniform distribution $\{1/3, 1/3, 1/3\}$. Also, we assume that the pedestrians have an uncertain intention with intents $\{\text{move fast, move slowly}\}$ subject to a uniform distribution $\{1/2, 1/2\}$. See Appx.-E for the detailed experimental configurations.

The turning task is first described as natural language. *The EV eventually reaches the target lane. Besides, the EV should only turn beyond the first pedestrian crossing and should always avoid collisions with the OV and the pedestrians at a risk level 0.05.* Then, the task is specified using a DSTL formula and converted to an STL formula (See Appx.-E) to facilitate a deterministic MPC problem as in Eq. (12). We consider a discrete-time $\Delta t = 0.5s$, a finite horizon $N = 36$, and a control cost $R = \text{diag}(1, 50)$. Similar to Case I, we update the linearized vehicle models using the most recent measurements before solving the optimization problem Eq. (12) at each time $k \in \{0, 1, \dots, N-1\}$ for the robustness against the linearization errors.

We use a comparison study to address the advantage of intention-aware control in risk restriction, where we consider two specifications that omit and incorporate the uncertain intentions of the OV and the pedestrians, respectively (See Appx.-E). The resulting trajectories of the vehicles and the pedestrians are shown in Fig. 5. The trajectories of the OV and the pedestrian are the results of 100 times Monte Carlo sampling. The multi-modal distribution of the OV is displayed, with each modal denoting the distribution of a *speeding-up*, a *constant-speed*, and a *slowing-down* intent,

respectively. We can see that the *no-awareness* EV is at risk of colliding with the OV for the *speeding-up* intent at time step $k = 16$. The multi-modal characteristics of the pedestrian are not obvious due to its low speed. But we can still see that *no-awareness* EV is at risk of colliding with the *moving-fast* pedestrians at time step $k = 20$. However, the intention-aware EV has successfully avoided collisions with all possible positions of the OV and the pedestrians by turning slightly earlier compared to the *no-awareness* case (See Fig. 5). Although this strategy seems antagonistic and aggressive from a practical perspective, it restricts the risk under the predefined level of 0.05. The results indicate that the developed intention-aware control method ensures restricted risk despite the complex joint uncertainties and linearization errors.

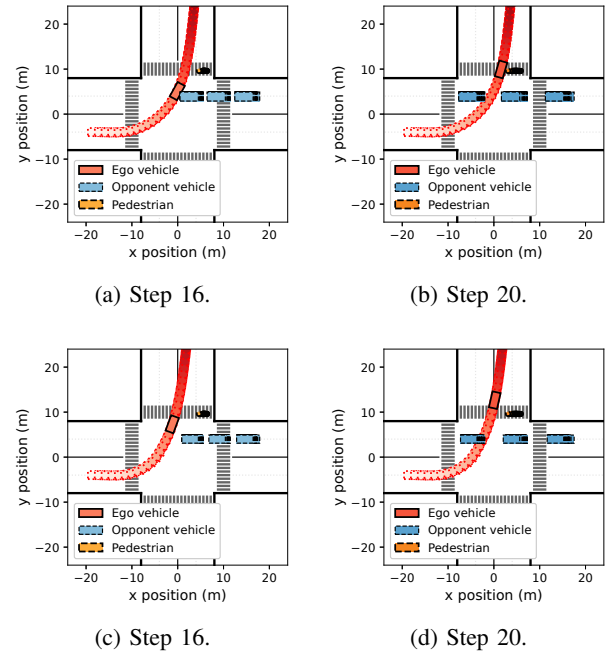


Fig. 5: Results of comparison study. (a) and (b): no awareness, the EV collides with the OV or with the pedestrians; (c) and (d): with intention awareness, no collisions occur.

The computation time per step for both *no-awareness* and *intention-awareness* scenarios is presented in Fig. 6. Both scenarios show exponentially decaying computation time as the step increases, implying the correctness of our analysis on computational complexity in Remark 2. It is noticed that the intention-aware controller involves heavier computation than the *no-awareness* one due to the incorporation of uncertain intentions. The computation is substantial before step 10 when the EV tries to find a feasible solution to avoid collisions with the OV and the pedestrians. The computation time before step 8 even exceeds the discrete sampling time 0.5s, bringing up a challenge to its deployment on a real-time system. Possible solutions to resolve this problem may include the decomposition [40], splitting [21], and conflict resolution [42] of STL specifications for a simplified task.

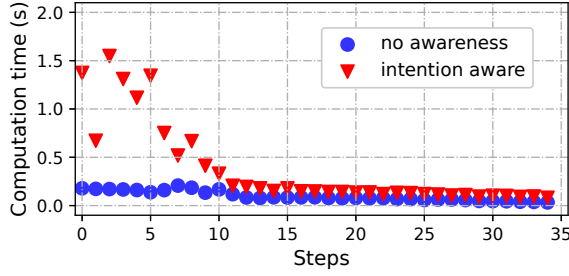


Fig. 6: The computation time per step (Case II).

V. CONCLUSIONS

This paper provides the first correct-by-design solution for intention-aware control of autonomous systems. This work has tackled the challenge of characterizing complex modeling-intention uncertainties using stochastic expansion, allowing solving an intention-, interaction-, and risk-aware controller using off-the-shelf tools. Experimental studies have validated the method's applicability to vehicle models with linearization errors. A limitation of this work is the heavy computational load for complex tasks, which will be resolved using specification simplification methods in future work. We will also investigate the extension of this work to sequential intention-aware control in the future.

APPENDIX

A. Signal Temporal Logic (STL)

For a discrete-time signal $\mathbf{s} := s_0 s_1 \dots$, where $s_k \in \mathbb{R}^n$ for $k \in \mathbb{N}$ and $n \in \mathbb{Z}^+$, the syntax of STL is given as [43]

$$\psi ::= \top \mid \mu \mid \neg \psi \mid \psi_1 \wedge \psi_2 \mid \psi_1 \cup_{[a,b]} \psi_2,$$

where ψ_1 , ψ_2 , and ψ are STL formulas, μ is a predicate with a mapping $h: \mathbb{R}^n \rightarrow \mathbb{R}$ via $\mu := \begin{cases} \top, & h(s_k) \geq 0 \\ \perp, & h(s_k) < 0 \end{cases}, k \in \mathbb{N}$. The *disjunction*, *eventually*, and *always* operators are defined as $\psi_1 \vee \psi_2 := \neg(\neg \psi_1 \wedge \neg \psi_2)$, $F_{[a,b]} \psi := \top \cup_{[a,b]} \psi$, $G_{[a,b]} \psi := \neg(\neg \top \cup_{[a,b]} \neg \psi)$. The semantics of STL denoted as $(\mathbf{s}, k) \models \psi$ are recursively determined as

$$\begin{aligned} (\mathbf{s}, k) \models \mu &\leftrightarrow h(s_k) \geq 0, \quad (\mathbf{s}, k) \models \neg \psi \leftrightarrow \neg((\mathbf{s}, k) \models \psi), \\ (\mathbf{s}, k) \models \psi_1 \wedge \psi_2 &\leftrightarrow (\mathbf{s}, k) \models \psi_1 \wedge (\mathbf{s}, k) \models \psi_2, \\ (\mathbf{s}, k) \models \psi_1 \vee \psi_2 &\leftrightarrow (\mathbf{s}, k) \models \psi_1 \vee (\mathbf{s}, k) \models \psi_2, \\ (\mathbf{s}, k) \models F_{[a,b]} \psi &\leftrightarrow \exists k' \in [k+a, k+b], \text{ s.t., } (\mathbf{s}, k') \models \psi, \\ (\mathbf{s}, k) \models G_{[a,b]} \psi &\leftrightarrow \forall k' \in [k+a, k+b], \text{ s.t., } (\mathbf{s}, k') \models \psi, \\ (\mathbf{s}, k) \models \psi_1 \cup_{[a,b]} \psi_2 &\leftrightarrow \exists k' \in [k+a, k+b], \text{ s.t., } (\mathbf{s}, k') \models \psi_2, \\ &\text{and } \forall k'' \in [k, k'], (\mathbf{s}, k'') \models \psi_1. \end{aligned}$$

For $k = 0$, the symbol k can be omitted, rendering $\mathbf{s} \models \psi$. The robustness of an STL formula ψ denoted as $\rho^\psi(\mathbf{s}, k)$, with

$\rho^\psi(\mathbf{s}, k) > 0 \leftrightarrow (\mathbf{s}, k) \models \psi$, is inductively defined as

$$\begin{aligned} \rho^\mu(\mathbf{s}, k) &:= h(s_k), \quad \rho^{\neg \psi}(\mathbf{s}, k) := -\rho^\psi(\mathbf{s}, k), \\ \rho^{\psi_1 \wedge \psi_2}(\mathbf{s}, k) &:= \min(\rho^{\psi_1}(\mathbf{s}, k), \rho^{\psi_2}(\mathbf{s}, k)), \\ \rho^{\psi_1 \vee \psi_2}(\mathbf{s}, k) &:= \max(\rho^{\psi_1}(\mathbf{s}, k), \rho^{\psi_2}(\mathbf{s}, k)), \\ \rho^{\psi_1 \cup_{[a,b]} \psi_2}(\mathbf{s}, k) &:= \max_{k' \in [k+a, k+b]} (\min(\rho^{\psi_2}(\mathbf{s}, k'), \\ &\quad \min_{k'' \in [k, k']} \rho^{\psi_1}(\mathbf{s}, k''))), \\ \rho^{F_{[a,b]} \psi}(\mathbf{s}, k) &:= \max_{k' \in [k+a, k+b]} \rho^\psi(\mathbf{s}, k'), \\ \rho^{G_{[a,b]} \psi}(\mathbf{s}, k) &:= \min_{k' \in [k+a, k+b]} \rho^\psi(\mathbf{s}, k'). \end{aligned}$$

For $k = 0$, the robustness reads $\rho^\psi(\mathbf{s})$.

B. Deterministic Model of EV

An autonomous vehicle is typically described as a nonlinear bicycle model [29], as illustrated in Fig. 7. Thus, we use the following deterministic model to describe the EV,

$$\text{EV} : \begin{cases} x_{k+1} = x_k + \Delta t v_k \cos(\theta_k + \gamma_k), \\ y_{k+1} = y_k + \Delta t v_k \sin(\theta_k + \gamma_k), \\ \theta_{k+1} = \theta_k + \Delta t v_k \sin \gamma_k / l, \\ v_{k+1} = v_k + \Delta t a_k, \end{cases} \quad (13)$$

where (x_k, y_k) denote the planar coordinate of the mass center of the front wheel at discrete time $k \in \mathbb{Z}$, θ_k and v_k are the heading angle of the vehicle and the linear velocity of the front wheel, respectively, γ_k , a_k are the steering angle and the linear acceleration of the front wheel, respectively, Δt is the discrete sampling time, and l is the length of the vehicle. Different from [29], all variables in Eq. (13) are defined for the front wheel instead of the mass center of the vehicle to obtain a simplified model. In fact, it is straightforward to convert Eq. (13) to a model for an arbitrary point on the vehicle. Let (x_k^a, y_k^a) , θ_k^a , and v_k^a be the planar coordinate, the heading angle, and the linear velocity of any mass point on the vehicle as shown in Fig. 7, their relations with the front wheel variables (x_k, y_k) , θ_k , and v_k are described by $x_k^a = x_k - (1-c)l \cos \theta_k$, $y_k^a = y_k - (1-c)l \sin \theta_k$, $v_k^a = v_k \cos \gamma_k / \cos \gamma_k^a$, and $\gamma_k^a = \tan^{-1}(c \tan \gamma_k)$, where $c \in [0, 1]$ is a ratio scalar such that cl is the distance from this point to the back wheel.

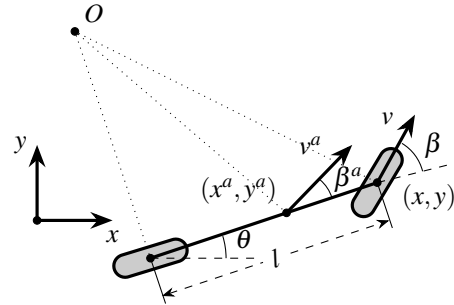


Fig. 7: The vehicle model.

Let $\xi_k = [x_k \ y_k \ \theta_k \ v_k]^\top$ be the state of the vehicle and $u_k = [\gamma_k \ a_k]^\top$ be the control input. The deterministic model of the EV is compactly represented as

$$\text{EV} : \begin{cases} \xi_{k+1} = \xi_k + f(\xi_k, u_k), \\ \zeta_k = \xi_k, \end{cases} \quad (14)$$

where $f(\xi_k, u_k) = \Delta t [v_k \cos(\theta_k + \gamma_k) \ v_k \sin(\theta_k + \gamma_k) \ \frac{v_k}{l} \sin \gamma_k \ a_k]^\top$. Here, we assume that all vehicle states are measurable. By linearizing Eq. (14) around $\zeta_0 = [x_0 \ y_0 \ \theta_0 \ v_0]^\top$ and $u_0 = [\gamma_0 \ a_0]^\top$, we obtain a linearized dynamic model,

$$f(\xi_k, u_k) = f(\zeta_0, u_0) + A(\zeta_0, u_0)(\xi_k - \zeta_0) + B(\zeta_0, u_0)(u_k - u_0),$$

where $A(\zeta_0, u_0) \in \mathbb{R}^{4 \times 4}$ and $B(\zeta_0, u_0) \in \mathbb{R}^{4 \times 2}$ are

$$A(\zeta_0, u_0) = \begin{bmatrix} 0 & 0 & -\Delta t v_0 \sin(\theta_0 + \gamma_0) & \Delta t \cos(\theta_0 + \gamma_0) \\ 0 & 0 & \Delta t v_0 \cos(\theta_0 + \gamma_0) & \Delta t \sin(\theta_0 + \gamma_0) \\ 0 & 0 & 0 & \Delta t \sin \gamma_0 / l \\ 0 & 0 & 0 & 0 \end{bmatrix},$$

$$B(\zeta_0, u_0) = \begin{bmatrix} -\Delta t v_0 \sin(\theta_0 + \gamma_0) & 0 \\ \Delta t v_0 \cos(\theta_0 + \gamma_0) & 0 \\ \Delta t v_0 \cos \gamma_0 / l & 0 \\ 0 & \Delta t \end{bmatrix}.$$

Assume $\theta_k \approx \theta_0$ for all $k \in \mathbb{Z}$ since a vehicle hardly performs large steering. With $\gamma_0 = 0$, we rewrite (14) as

$$\text{EV} : \begin{cases} \xi_{k+1} = A_0 \xi_k + B_0 u_k + \varepsilon_0, \\ \zeta_k = \xi_k, \end{cases} \quad (15)$$

where

$$A_0 = I + \Delta t \begin{bmatrix} 0 & 0 & -v_0 \sin \theta_0 & \cos \theta_0 \\ 0 & 0 & v_0 \cos \theta_0 & \sin \theta_0 \\ 0 & 0 & 0 & 0 \\ 0 & 0 & 0 & 0 \end{bmatrix},$$

$$B_0 = \Delta t \begin{bmatrix} -v_0 \sin \theta_0 & 0 \\ v_0 \cos \theta_0 & 0 \\ 0 & 0 \\ 0 & 1 \end{bmatrix}, \text{ and } \varepsilon_0 = \Delta t \begin{bmatrix} v_0 \theta_0 \sin \theta_0 \\ -v_0 \theta_0 \cos \theta_0 \\ 0 \\ 0 \end{bmatrix}.$$

C. Stochastic Model of an OV and the PCE Model

Based on Appx.-B, we use a stochastic bicycle model to describe the behavior of an OV with uncertain parameters,

$$\text{OV} : \begin{cases} x_{k+1} = x_k + \Delta t v_k \cos(\theta_k + \gamma_k), \\ y_{k+1} = y_k + \Delta t v_k \sin(\theta_k + \gamma_k), \\ \theta_{k+1} = \theta_k + \Delta t v_k \sin \gamma_k / l, \\ v_{k+1} = v_k + \Delta t (a_k + \delta), \end{cases} \quad (16)$$

where $l \sim p_l$ is the unknown length of the vehicle and $\delta \sim p_\delta$ is a random acceleration control offset, where p_l and p_δ are known PDFs. We assume an integer-valued intention variable $\iota \in I \subset \mathbb{Z}$ with a distribution p_ι on I and an intention-encoding feedforward controller $u_k = \iota \tau_k$ for the OV, where $u_k = [\gamma_k, a_k]^\top$ is the control input of the OA and $\tau_k \in \mathbb{R}^2$ for $k \in \mathbb{N}$ is a known control signal. Supposing that the feedforward control input τ_0, τ_1, \dots is designed such that $u_k = \tau_k$ leads to an accelerating OV, the intents $\iota = -1, 0, 1$ encode the *slowing-down*, *constant-speed*, and *speeding-up* driving policies, respectively.

By linearizing the OV dynamic model similar to Appx.-B, we obtain the following linearized stochastic model,

$$\text{OV} : \begin{cases} \xi_{k+1} = A_0 \xi_k + \sum_{i=0}^1 b_i(\eta) B_i \tau_k + \sum_{i=0}^1 e_i(\eta) \varepsilon_i, \\ \zeta_k = \xi_k, \end{cases} \quad (17)$$

where $\eta = [l \ \delta \ \iota]^\top$ is a joint random variable, $b_0(\eta) = \iota$, $b_1(\eta) = \iota/l$, $e_0(\eta) = 1$, and $e_1(\eta) = \delta$, A_0 , B_0 , and ε_0 are given in Appx.-B, and

$$B_1 = \Delta t \begin{bmatrix} 0 & 0 \\ 0 & 0 \\ v_0 \cos \theta_0 & 0 \\ 0 & 0 \end{bmatrix} \text{ and } \varepsilon_1 = \Delta t \begin{bmatrix} 0 \\ 0 \\ 0 \\ 1 \end{bmatrix}. \quad (18)$$

We use PCE to expand the state and uncertain parameters of Eq. (17) as $\xi_k = \sum_{j=0}^{L-1} \hat{\xi}_{k,j} \Phi_j$ for $k \in \mathbb{N}$, $b_0(\eta) = \hat{\mathbf{b}}_0^\top \Phi$, $b_1(\eta) = \hat{\mathbf{b}}_1^\top \Phi$, $e_0(\eta) = \hat{\mathbf{e}}_0^\top \Phi$, $e_1(\eta) = \hat{\mathbf{e}}_1^\top \Phi$, where $\Phi = [\Phi_0, \Phi_1, \dots, \Phi_{L-1}]^\top$ is the polynomial bases of the joint uncertainty η with $\Phi_0 := 1$, $\hat{\xi}_{k,j} \in \mathbb{R}$ for $j = 0, 1, \dots, L-1$ and $\hat{\mathbf{b}}_0, \hat{\mathbf{b}}_1, \hat{\mathbf{e}}_0, \hat{\mathbf{e}}_1 \in \mathbb{R}^L$ are vectors of PCE coefficients. Substituting the expansions above to Eq. (17) renders

$$\sum_{j=0}^{L-1} \hat{\xi}_{k+1,j} \Phi_j = A_0 \sum_{j=0}^{L-1} \hat{\xi}_{k,j} \Phi_j + \sum_{i=0}^1 \hat{\mathbf{b}}_i^\top \Phi B_i \tau_k + \sum_{i=0}^1 \hat{\mathbf{e}}_i^\top \Phi \varepsilon_i.$$

Taking the inner product of both sides with any polynomial bases Φ_s , $s \in \{0, 1, \dots, L-1\}$, we have

$$\sum_{j=0}^{L-1} \hat{\xi}_{k+1,j} \langle \Phi_j, \Phi_s \rangle = \sum_{j=0}^{L-1} A_0 \hat{\xi}_{k,j} \langle \Phi_j, \Phi_s \rangle + \sum_{i=0}^1 \hat{\mathbf{b}}_i^\top \langle \Phi, \Phi_s \rangle B_i \tau_k + \sum_{i=0}^1 \hat{\mathbf{e}}_i^\top \langle \Phi, \Phi_s \rangle \varepsilon_i.$$

The orthogonal properties of the bases ensure $\langle \Phi_s, \Phi_s \rangle > 0$, $\forall s \in \{0, 1, \dots, N-1\}$ and $\langle \Phi_j, \Phi_s \rangle = 0$, $\forall j, s \in \{0, 1, \dots, L-1\}$, $j \neq s$. The PCE model of the OV reads

$$\begin{aligned} \hat{\xi}_{k+1} &= \mathbf{A} \hat{\xi}_k + \mathbf{B} \tau_k + \boldsymbol{\varepsilon}, \\ \hat{\zeta}_k &= \hat{\xi}_k, \end{aligned} \quad (19)$$

where $\hat{\xi}_k = [\hat{\xi}_{k,0}^\top \ \hat{\xi}_{k,1}^\top \ \dots \ \hat{\xi}_{k,L-1}^\top]^\top$, $\mathbf{A} = \text{diag}(A_0, \dots, A_0)$,

$$\mathbf{B} = \begin{bmatrix} \sum_{i=0}^1 \hat{b}_{i,0} B_i \\ \sum_{i=0}^1 \hat{b}_{i,1} B_i \\ \vdots \\ \sum_{i=0}^1 \hat{b}_{i,L-1} B_i \end{bmatrix}, \text{ and } \boldsymbol{\varepsilon} = \begin{bmatrix} \sum_{i=0}^1 \hat{e}_{i,0} \varepsilon_i \\ \sum_{i=0}^1 \hat{e}_{i,1} \varepsilon_i \\ \vdots \\ \sum_{i=0}^1 \hat{e}_{i,L-1} \varepsilon_i \end{bmatrix}.$$

with an initial condition $\hat{\xi}_0 = [\xi_0^\top \ \underbrace{\mathbf{0}_{4 \times 1}^\top \ \dots \ \mathbf{0}_{4 \times 1}^\top}_{L-1}]^\top$, where

$\hat{b}_{i,j}$ and $\hat{e}_{i,j}$ are the j -th element of vectors $\hat{\mathbf{b}}_i$ and $\hat{\mathbf{e}}_i$, for $i \in \{0, 1\}$ and $j \in \{0, 1, \dots, L-1\}$.

D. Configuration of Case I

Case I considers a deterministic EV model given in Appx.-B, with a deterministic state variable $\zeta_k^E \in \mathbb{R}^4$ and a stochastic OV model given in Appx.-C, with a stochastic state variable $\zeta_k^O \in \mathbb{R}^4$. The elements of the variables, i.e., $\zeta_{i,k}^E$ and $\zeta_{i,k}^O$ for $i \in \{1, 2, 3, 4\}$ denote the longitudinal positions, the latitudinal positions, the orientations, and the linear velocities of the EV and the OV, respectively.

Following the natural language description in Sec. IV-A, the overtaking task is specified as DSTL predicates: *The EV eventually switches to the slow lane* ($(v_1^E, *) := |\zeta_{2,k}^E - l_{\text{slow}}| < 0.1m \wedge |\zeta_{3,k}^E| < 0.1\text{rad}$) and *drives in front of the OV at a maximal risk level 0.05* ($(v_2^E, 0.05) := P(\zeta_{1,k}^O \leq \zeta_{1,k}^E - d_{\text{safe},1}) \geq$

0.95), if the OV does not switch to the fast lane ($(v_1^O, 1) := \mu_{w_{2,k}} < l_{\text{mid}}$) or exceed a speed limit v_{lim} ($(v_2^O, 1) := \mu_{w_{4,k}} < v_{\text{lim}}$). Meanwhile, the EV should always drive inside the lanes ($(v_1^S, *) := l_{\text{bot}} < \zeta_{2,k}^E \leq l_{\text{top}}$) and keep a minimal distance with the OV, $d_{\text{safe},x} = 10\text{m}$ longitudinally and $d_{\text{safe},y} = 2\text{m}$ latitudinally, at a maximal risk level 0.05 ($(v_2^S, 0.05) := P(|\zeta_{1,k}^O - \zeta_{1,k}^E| < d_{\text{safe},x} \wedge |\zeta_{2,k}^O - \zeta_{2,k}^E| < d_{\text{safe},y}) \geq 0.95$). Here, $*$ denotes an arbitrary value in $[0, 1]$. Then, this task is specified as $\varphi := G_{[0,N]} \bigwedge_{j=1}^2 (v_j^S, 0.05) \wedge (G_{[0,N]} \bigwedge_{j=1}^2 (v_j^O, 1) \rightarrow F_{[0,N-3]} G_{[0,3]} \bigwedge_{j=1}^2 (v_j^E, 0.05))$. Using Eq. (11), we convert the DSTL formula φ into an STL formula.

E. Configuration of Case II

Case II considers a deterministic EV model given in Appx.-B, with a deterministic state variable $\zeta_k^E \in \mathbb{R}^4$ and a stochastic OV model given in Appx.-C, with a stochastic state variable $\zeta_k^O \in \mathbb{R}^4$. Besides, we use another stochastic OV model to denote the dynamics of a group of pedestrians, with a stochastic state variable $\zeta_k^P \in \mathbb{R}^4$. The elements of these variables, i.e., $\zeta_{i,k}^E$, $\zeta_{i,k}^O$, and $\zeta_{i,k}^P$ for $i \in \{1, 2, 3, 4\}$ denote the longitudinal positions, the latitudinal positions, the orientations, and the linear velocities of the EV, the OV, and the pedestrian, respectively.

Following the natural language description in Sec. IV-B, the turning task is specified as DSTL predicates: *The EV eventually reaches the target lane* ($(v_1^E, *) := |\zeta_{1,k}^E - l/2| < 0.1\text{m} \wedge \zeta_{2,k}^E > 3l/2$). *Besides, the EV should only turn after the first pedestrian crossing* ($(v_2^E, *) : (\zeta_{1,k}^E < -1.2l) \rightarrow (|\zeta_{2,k}^E + l/2| < 0.1\text{m})$) and *should always avoid collisions with the OV and the pedestrians at a risk level 0.05* ($(v_1^S, 0.05) := P(|\zeta_{1,k}^O - \zeta_{1,k}^E| < d_{\text{safe},x}^O \wedge |\zeta_{2,k}^O - \zeta_{2,k}^E| < d_{\text{safe},y}^O) \geq 0.95$ and $(v_2^S, 0.05) := P(|\zeta_{1,k}^P - \zeta_{1,k}^E| < d_{\text{safe},x}^P \wedge |\zeta_{2,k}^P - \zeta_{2,k}^E| < d_{\text{safe},y}^P) \geq 0.95$). Here, $*$ denotes an arbitrary value in $[0, 1]$, $l = 8\text{m}$ is the width of each lane, and $d_{\text{safe},i}^O = 4\text{m}$ and $d_{\text{safe},i}^P = 2\text{m}$ are safe distances between the EV and the OV and the pedestrians, respectively, for $i \in \{x, y\}$ representing the longitudinal and latitudinal directions, respectively.

The intention-aware DSTL specification for the task is $\varphi := (G_{[0,N]} \bigwedge_{j=1}^2 (v_j^S, 0.05)) \wedge (F_{[0,N-3]} G_{[0,3]} \bigwedge_{j=1}^2 (v_j^E, *))$. The no-intention one is $\varphi' := (F_{[0,N-3]} G_{[0,3]} \bigwedge_{j=1}^2 (v_j^E, *))$. Using Eq. (11), we convert these DSTL formulas into STL formulas for the comparison study.

REFERENCES

- [1] J. S. Park, C. Park, and D. Manocha, "I-planner: Intention-aware motion planning using learning-based human motion prediction," *The International Journal of Robotics Research*, vol. 38, no. 1, pp. 23–39, 2019.
- [2] X. Wu, R. Chandra, T. Guan, A. Bedi, and D. Manocha, "Intention-aware planning in heterogeneous traffic via distributed multi-agent reinforcement learning," in *Conference on Robot Learning*. PMLR, 2023, pp. 446–477.
- [3] B. Varga, D. Yang, and S. Hohmann, "Intention-aware decision-making for mixed intersection scenarios," in *2023 IEEE 17th International Symposium on Applied Computational Intelligence and Informatics (SACI)*. IEEE, 2023, pp. 000 369–000 374.
- [4] H. Bai, S. Cai, N. Ye, D. Hsu, and W. S. Lee, "Intention-aware online POMDP planning for autonomous driving in a crowd," in *2015 IEEE International Conference on Robotics and Automation (ICRA)*. IEEE, 2015, pp. 454–460.

- [5] T. Bandyopadhyay, K. S. Won, E. Frazzoli, D. Hsu, W. S. Lee, and D. Rus, "Intention-aware motion planning," in *Algorithmic Foundations of Robotics X: Proceedings of the Tenth Workshop on the Algorithmic Foundations of Robotics*. Springer, 2013, pp. 475–491.
- [6] S. Qi and S.-C. Zhu, "Intent-aware multi-agent reinforcement learning," in *2018 IEEE International Conference on Robotics and Automation (ICRA)*. IEEE, 2018, pp. 7533–7540.
- [7] W. Zhao, J. P. Queralta, and T. Westerlund, "Sim-to-real transfer in deep reinforcement learning for robotics: A survey," in *2020 IEEE Symposium Series on Computational Intelligence (SSCI)*. IEEE, 2020, pp. 737–744.
- [8] X. Li, Z. Serlin, G. Yang, and C. Belta, "A formal methods approach to interpretable reinforcement learning for robotic planning," *Science Robotics*, vol. 4, no. 37, p. eaay6276, 2019.
- [9] C.-J. Hoel, K. Wolff, and L. Laine, "Ensemble quantile networks: Uncertainty-aware reinforcement learning with applications in autonomous driving," *IEEE Transactions on Intelligent Transportation Systems*, 2023.
- [10] A. Salamati, S. Soudjani, and M. Zamani, "Data-driven verification of stochastic linear systems with signal temporal logic constraints," *Automatica*, vol. 131, p. 109781, 2021.
- [11] T. Badings, L. Romao, A. Abate, and N. Jansen, "Probabilities are not enough: Formal controller synthesis for stochastic dynamical models with epistemic uncertainty," in *Proceedings of the AAAI Conference on Artificial Intelligence*, vol. 37, no. 12, 2023, pp. 14 701–14 710.
- [12] M. H. W. Engelaar, Z. Zhang, M. Lazar, and S. Haesaert, "Risk-aware MPC for stochastic systems with runtime temporal logics," *arXiv preprint arXiv:2402.03165*, 2024.
- [13] S. S. Farahani, R. Majumdar, V. S. Prabhu, and S. Soudjani, "Shrinking horizon model predictive control with signal temporal logic constraints under stochastic disturbances," *IEEE Transactions on Automatic Control*, vol. 64, no. 8, pp. 3324–3331, 2018.
- [14] S. Haesaert, P. Nilsson, C. I. Vasile, R. Thakker, A.-a. Aghamohammadi, A. D. Ames, and R. M. Murray, "Temporal logic control of POMDPs via label-based stochastic simulation relations," *IFAC-PapersOnLine*, vol. 51, no. 16, pp. 271–276, 2018.
- [15] D. N. Jansen, F. Nielson, and L. Zhang, "Belief bisimulation for hidden Markov models: Logical characterisation and decision algorithm," in *NASA Formal Methods: 4th International Symposium, NFM 2012, Norfolk, VA, USA, April 3-5, 2012. Proceedings 4*. Springer, 2012, pp. 326–340.
- [16] A. Jones, M. Schwager, and C. Belta, "Distribution temporal logic: Combining correctness with quality of estimation," in *52nd IEEE Conference on Decision and Control*. IEEE, 2013, pp. 4719–4724.
- [17] K. Leahy, E. Cristofalo, C.-I. Vasile, A. Jones, E. Montijano, M. Schwager, and C. Belta, "Control in belief space with temporal logic specifications using vision-based localization," *The International Journal of Robotics Research*, vol. 38, no. 6, pp. 702–722, 2019.
- [18] D. Sadigh and A. Kapoor, "Safe control under uncertainty with probabilistic signal temporal logic," in *Proceedings of Robotics: Science and Systems XII*, 2016.
- [19] T. A. N. Heirung, J. A. Paulson, J. O'Leary, and A. Mesbah, "Stochastic model predictive control—how does it work?" *Computers & Chemical Engineering*, vol. 114, pp. 158–170, 2018.
- [20] K. Leahy, A. Jones, and C.-I. Vasile, "Fast decomposition of temporal logic specifications for heterogeneous teams," *IEEE Robotics and Automation Letters*, vol. 7, no. 2, pp. 2297–2304, 2022.
- [21] Z. Zhang and S. Haesaert, "Modularized control synthesis for complex signal temporal logic specifications," in *2023 62nd IEEE Conference on Decision and Control (CDC)*. IEEE, 2023, pp. 7856–7861.
- [22] L. Lindemann, M. Cleaveland, G. Shim, and G. J. Pappas, "Safe planning in dynamic environments using conformal prediction," *IEEE Robotics and Automation Letters*, 2023.
- [23] M. S. Eldred and H. C. Elman, "Design under uncertainty employing stochastic expansion methods," *International Journal for Uncertainty Quantification*, vol. 1, no. 2, 2011.
- [24] L. Dai, Y. Xia, and Y. Gao, "Distributed model predictive control of linear systems with stochastic parametric uncertainties and coupled probabilistic constraints," *SIAM Journal on Control and Optimization*, vol. 53, no. 6, pp. 3411–3431, 2015.
- [25] A. Der Kiureghian and O. Ditlevsen, "Aleatory or epistemic? Does it matter?" *Structural Safety*, vol. 31, no. 2, pp. 105–112, 2009.
- [26] V. Kurtz and H. Lin, "Mixed-integer programming for signal temporal logic with fewer binary variables," *IEEE Control Systems Letters*, vol. 6, pp. 2635–2640, 2022.

- [27] N. Dang, T. Shi, Z. Zhang, W. Jin, M. Leibold, and M. Buss, "Identifying reaction-aware driving styles of stochastic model predictive controlled vehicles by inverse reinforcement learning," in *2023 IEEE 26th International Conference on Intelligent Transportation Systems (ITSC)*. IEEE, 2023, pp. 2887–2892.
- [28] V. Lefkopoulos, M. Menner, A. Domahidi, and M. N. Zeilinger, "Interaction-aware motion prediction for autonomous driving: A multiple model Kalman filtering scheme," *IEEE Robotics and Automation Letters*, vol. 6, no. 1, pp. 80–87, 2020.
- [29] J. Kong, M. Pfeiffer, G. Schildbach, and F. Borrelli, "Kinematic and dynamic vehicle models for autonomous driving control design," in *2015 IEEE Intelligent Vehicles Symposium (IV)*. IEEE, 2015, pp. 1094–1099.
- [30] R. P. Rao, "Decision making under uncertainty: a neural model based on partially observable Markov decision processes," *Frontiers in Computational Neuroscience*, vol. 4, p. 146, 2010.
- [31] H. Ahn, C. Chen, I. M. Mitchell, and M. Kamgarpour, "Safe motion planning against multimodal distributions based on a scenario approach," *IEEE Control Systems Letters*, vol. 6, pp. 1142–1147, 2021.
- [32] Y. Xing, C. Lv, H. Wang, H. Wang, Y. Ai, D. Cao, E. Velenis, and F.-Y. Wang, "Driver lane change intention inference for intelligent vehicles: Framework, survey, and challenges," *IEEE Transactions on Vehicular Technology*, vol. 68, no. 5, pp. 4377–4390, 2019.
- [33] B. Gangopadhyay, S. Khastgir, S. Dey, P. Dasgupta, G. Montana, and P. Jennings, "Identification of test cases for automated driving systems using Bayesian optimization," in *2019 IEEE Intelligent Transportation Systems Conference (ITSC)*. IEEE, 2019, pp. 1961–1967.
- [34] A. M. McKeand, R. M. Gorguluarslan, and S.-K. Choi, "Stochastic analysis and validation under aleatory and epistemic uncertainties," *Reliability Engineering & System Safety*, vol. 205, p. 107258, 2021.
- [35] T. Brüdigam, M. Olbrich, D. Wollherr, and M. Leibold, "Stochastic model predictive control with a safety guarantee for automated driving," *IEEE Transactions on Intelligent Vehicles*, 2021.
- [36] L. Fagiano and M. Khammash, "Nonlinear stochastic model predictive control via regularized polynomial chaos expansions," in *2012 IEEE 51st IEEE Conference on Decision and Control (CDC)*. IEEE, 2012, pp. 142–147.
- [37] G. C. Calafiore and L. E. Ghaoui, "On distributionally robust chance-constrained linear programs," *Journal of Optimization Theory and Applications*, vol. 130, pp. 1–22, 2006.
- [38] F. Petzke, A. Mesbah, and S. Streif, "Pocet: a polynomial chaos expansion toolbox for matlab," *IFAC-PapersOnLine*, vol. 53, no. 2, pp. 7256–7261, 2020.
- [39] T. Crestaux, O. Le Maître, and J.-M. Martinez, "Polynomial chaos expansion for sensitivity analysis," *Reliability Engineering & System Safety*, vol. 94, no. 7, pp. 1161–1172, 2009.
- [40] M. Charitidou and D. V. Dimarogonas, "Signal temporal logic task decomposition via convex optimization," *IEEE Control Systems Letters*, vol. 6, pp. 1238–1243, 2021.
- [41] J. Feinberg, V. G. Eck, and H. P. Langtangen, "Multivariate polynomial chaos expansions with dependent variables," *SIAM Journal on Scientific Computing*, vol. 40, no. 1, pp. A199–A223, 2018.
- [42] T. Yang, Y. Zou, S. Li, and Y. Yang, "Distributed model predictive control for probabilistic signal temporal logic specifications," *IEEE Transactions on Automation Science and Engineering*, 2023.
- [43] A. Donzé, "On signal temporal logic," in *Runtime Verification: 4th International Conference, RV 2013, Rennes, France, September 24–27, 2013. Proceedings 4*. Springer, 2013, pp. 382–383.